Effects of Vertical Wind Shear on the Predictability of Tropical Cyclones

FUQING ZHANG AND DANDAN TAO

Department of Meteorology, The Pennsylvania State University, University Park, Pennsylvania

ABSTRACT

Through cloud-resolving simulations, this study examines the effect of vertical wind shear and system-scale flow asymmetry on the predictability of tropical cyclone (TC) intensity during different stages of the TC life cycle. A series of ensemble experiments is performed with varying magnitudes of vertical wind shear, each initialized with an idealized weak TC-like vortex, with small-scale, small-amplitude random perturbations added to the initial conditions. It is found that the environmental shear can significantly affect the intrinsic predictability of tropical cyclones, especially during the formation and rapid intensification stage. The larger the vertical wind shear, the larger the uncertainty in the intensity forecast, primarily owing to the difference in the timing of rapid intensification.

In the presence of environmental shear, initial random noise may result in changes in the timing of rapid intensification by as much as 1–2 days through the randomness (and chaotic nature) of moist convection. Upscale error growth from differences in moist convection first alters the tilt amplitude and angle of the incipient tropical storms, which leads to significant differences in the timing of precession and vortex alignment. During the precession process, both the vertical tilt of the storm and the effective (local) vertical wind shear are considerably decreased after the tilt angle reaches 90° to the left of the environmental shear. The tropical cyclone intensifies immediately after the tilt and the effective local shear reach their minima. In some instances, small-scale, small-amplitude random noise may also limit the intensity predictability through altering the timing and strength of the eyewall replacement cycle.

1. Introduction

For the past few decades, despite large improvement in the track forecast of tropical cyclones (TCs), there is almost no improvement in the intensity forecast for all lead times (Cangialosi and Franklin 2012). This is due not only to the fact that hurricane intensity may be intrinsically less predictable than the track forecast, but also because of deficiencies in the forecast models or in the initial conditions that are used to produce the forecasts. The current-generation operational models for hurricane intensity prediction still lack sufficient grid spacing, initialize tropical cyclones without the incorporation of inner-core observations, and use inefficient data assimilation methods. A recent study by Zhang et al. (2011) showed that the hurricane intensity forecast accuracy can be improved by as much as 30%–40% through convection-permitting ensemble simulations that assimilate

airborne Doppler radar observations within the inner-core area with an advanced data assimilation method.

Compared to track, which is more dependent on the environmental conditions, tropical cyclone intensity can be more strongly dependent on internal dynamics and moist convection, which occur on smaller scales, and are more chaotic, less well understood, and intrinsically less predictable. The recent study of Zhang and Sippel (2009) showed that small initial-condition errors can lead to very different intensity forecasts owing to the presence of moist convection. This suggests that at least for some storms the intensity forecasts may be intrinsically limited. This effect of moist convection in limiting predictability has also been seen for the mesoscale structure of midlatitude extratropical cyclones (Zhang et al. 2002, 2003, 2007). The limited predictability of tropical cyclones has also been examined in the recent studies of Sippel and Zhang (2008, 2010) and Nguyen et al. (2008, hereafter NSM08). For example, NSM08 found that small random moisture perturbations in the boundary layer might greatly change the flow asymmetry owing to the abundance of deep convective vortex structures. They further concluded that the deterministic prediction of

Corresponding author address: Fuqing Zhang, Department of Meteorology, The Pennsylvania State University, University Park, PA 16802.
E-mail: fzhang@psu.edu

maximum intensity using either maximum wind or minimum surface pressure metrics has large intrinsic uncertainty.

This current study examines the effect of vertical wind shear and system-scale flow asymmetry on the predictability of tropical cyclone intensity during different stages of the TC life cycle (i.e., initial formation, rapid intensification, and quasi-steady mature phase). Vertical wind shear has long been recognized to have a strong influence on the development, structure, and intensity of tropical cyclones (e.g., Tang and Emanuel 2010; Molinari and Vollaro 2010; Rappin and Nolan 2012; Deng et al. 2012; and references therein), but to the best of our knowledge, its influence on the predictability of tropical cyclones has never been explored in literature. We first begin by evaluating the validity of the NSM08 findings under environmental conditions with no mean flow and no background shear, using a more modern numerical weather prediction model with higher model resolution and better physics parameterizations. We then proceed by examining the intensity forecast sensitivity to small-scale, small-amplitude moisture perturbations as in NSM08, but under weak to moderate environmental vertical wind shear.

2. Experimental design

The Advanced Research version of the Weather Research and Forecast (ARW-WRF) model, version 3.1.1, is used for all the simulations. There are three two-way nested model domains, with domain sizes of 4320 km × 4320 km (D1), 1440 km × 1440 km (D2), and 720 km × 720 km (D3), and horizontal grid spacings of 18, 6, and 2 km, respectively. The model has 41 vertical levels with the model top at 20 km. The two nested domains (D2 and D3) are moveable, with the domain center following the 850-hPa center of the tropical cyclones. The model uses the Yonsei University (YSU) boundary layer scheme (Hong et al. 2006) with a surface layer scheme of Dudhia et al. (2008) (isftcflx = 1 in WRF), WRF single-moment 6-class (WSM6) microphysics (Hong and Lim 2006), and no cumulus parameterization. All simulations are initialized with the same idealized modified Rankine vortex but with different distributions of random low-level moisture perturbations. The initial vortices have a maximum azimuthal-mean surface wind speed of 15 m s^{-1} at 135-km radius. The "moist tropical" mean hurricane season sounding of Dunion and Marron (2008) is used for the environmental moisture and temperature profile, while a constant sea surface temperature of 27°C and a constant Coriolis parameter equivalent to 20°N are used.

There are four sets of ensemble experiments, each with 20 members. Different moisture perturbations with
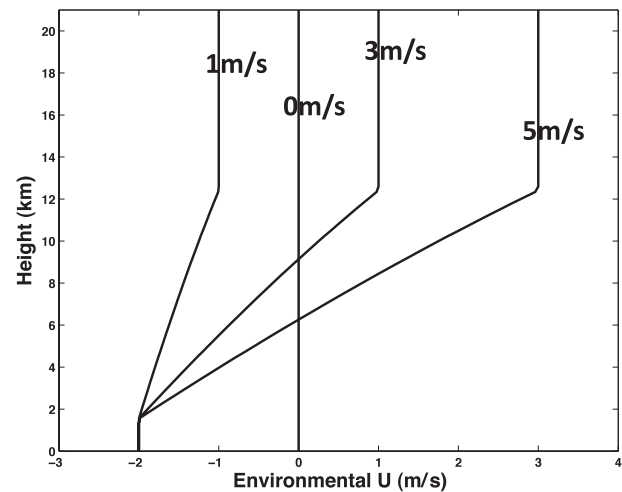

FIG. 1. Vertical profiles of environmental flow for SH0 (0 m s^{-1} vertical wind shear), SH1 (1 m s^{-1}), SH3 (3 m s^{-1}), and SH5 (5 m s^{-1}).

the magnitude randomly selected from a uniform distribution of $(-0.5, 0.5)$ g kg^{-1} are applied to the water vapor mixing ratio throughout the innermost domain below 950 hPa. The initial vortex, the environmental conditions, and the initial moisture perturbations follow closely the recent study of NSM08, which examined the predictability of tropical cyclones under quiescent (no mean flow) conditions with coarser resolution and less sophisticated model physics configurations using the fifth-generation Pennsylvania State University (PSU)–National Center for Atmospheric Research (NCAR) Mesoscale Model (MM5). The vertical profiles of the environmental flow for all ensemble experiments are shown in Fig. 1. There is no environmental mean flow or vertical wind shear in ensemble experiment "SH0," as in NSM08. The other three experiments (namely, "SH1," "SH3," and "SH5") have westerly vertical wind shear of 1, 3, and 5 m s^{-1}, respectively, but all have the same surface mean easterly wind of 2 m s^{-1}. The "point downscaling" method developed by Nolan (2011) is used to add the vertical shear (with no temperature gradient) in these idealized simulations. Another ensemble experiment with no shear but with 2 m s^{-1} mean easterly wind is also performed but since there is no systematic difference from the results of SH0, the results from this additional no-shear experiment will not be further discussed here for brevity.

3. Results

a. Forecast uncertainty versus vertical wind shear

Figure 2 shows the time evolution of the tropical cyclone intensity in terms of the 10-m maximum wind
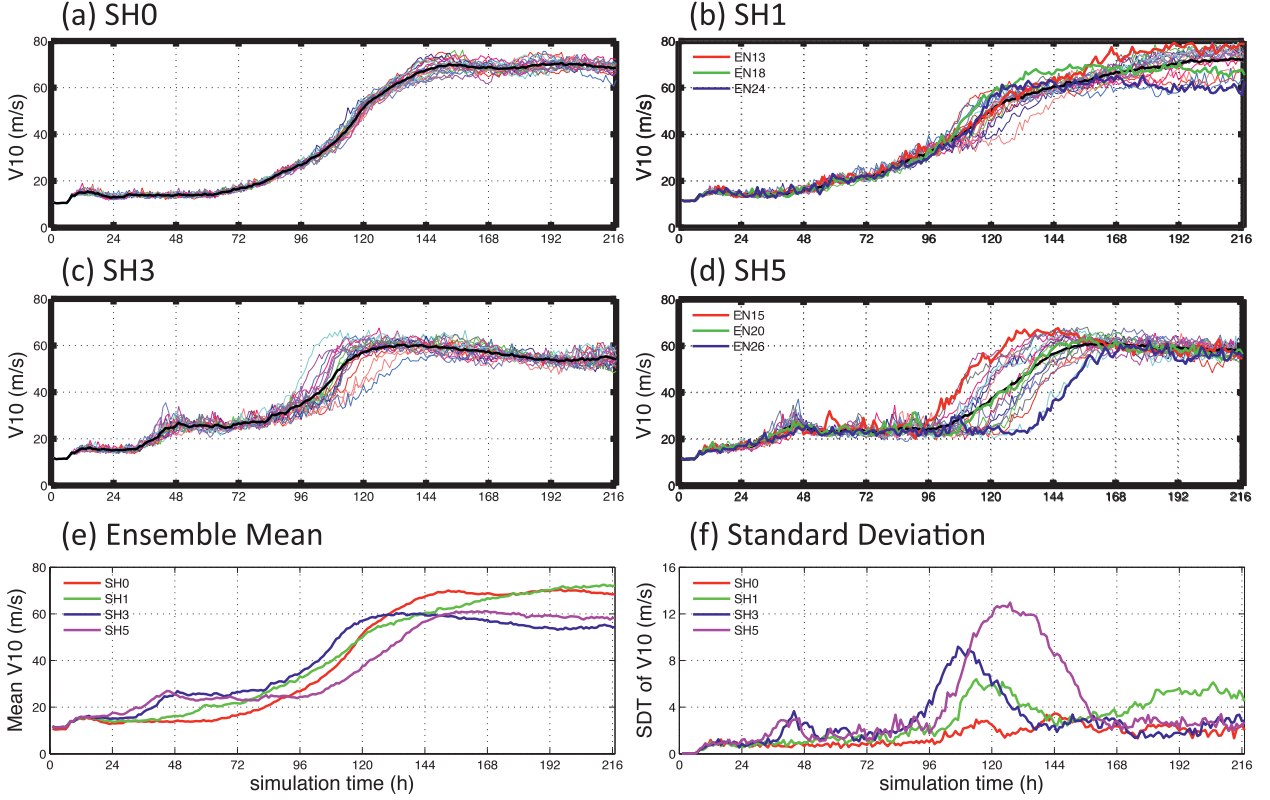
FIG. 2. Time evolution of the tropical cyclone intensity in terms of the 10-m maximum wind speed for all ensemble members of (a) SH0, (b) SH1, (c) SH3, (d) SH5, along with (e) the ensemble mean and (f) the standard deviation (ensemble spread) from all ensemble experiments. The thick black lines in (a)–(d) denote the ensemble mean, while EN13, EN18, and EN24 of SH1 in (b) and EN15, EN20, and EN26 of SH5 in (d) are denoted with thick colored lines.

speed along with the mean and standard deviation (ensemble spread) from all ensemble experiments under different environmental flow conditions (with and without vertical wind shear). We can see increasingly larger intensity forecast divergence among ensemble members for experiments with increasingly stronger vertical wind shear. In particular, the following can be noted: 1) the intensity forecast uncertainty is greatest during the rapid intensification (RI) stage of the tropical cyclones; 2) the larger the vertical shear, the larger the ensemble spread[1] during the RI stage; and 3) after the completion of RI, the ensemble spread becomes similar (and smaller) among different groups of ensembles except for SH1 (for reasons to be discussed in section 3c).

During RI, the largest ensemble spread of intensity is nearly 13 m s^{-1} in SH5 (with the largest shear of 5 m s^{-1}), which is nearly 4 times larger than the maximum ensemble spread of intensity ($\sim$3 m s^{-1}) in SH0. The maximum ensemble spread is about 9 m s^{-1} in SH3 and about 6 m s^{-1} in SH1. The difference between experiments SH0 and SH1 suggests that even the slightest vertical wind shear may considerably increase the forecast uncertainty and thus further limit the predictability of tropical cyclones. This also suggests that past predictability studies of tropical cyclones with no environmental shear such as NSM08 may not be representative of real-world tropical cyclones. On the other hand, although our experimental design in SH0 follows closely NSM08 by using a similar initial vortex and the same-amplitude boundary layer moisture perturbations, the ensemble spread in SH0 is considerably smaller than (less than half) that obtained in NSM08. The larger forecast uncertainty by NSM08 might be due to their use of a different (less state of the science) forecast model with simpler physics and their use of a much-coarser grid resolution in both the horizontal and the vertical. It is

---

[1] Note that as in NSM08 the instantaneous model output is used for the tropical cyclone intensity in terms of peak wind or minimum sea level pressure. This may lead to a larger ensemble spread than for a 3- or 6-h running mean. Refer to Uhlhorn and Nolan (2012) for more on the issue of sampling and representativeness for tropical cyclone intensity.
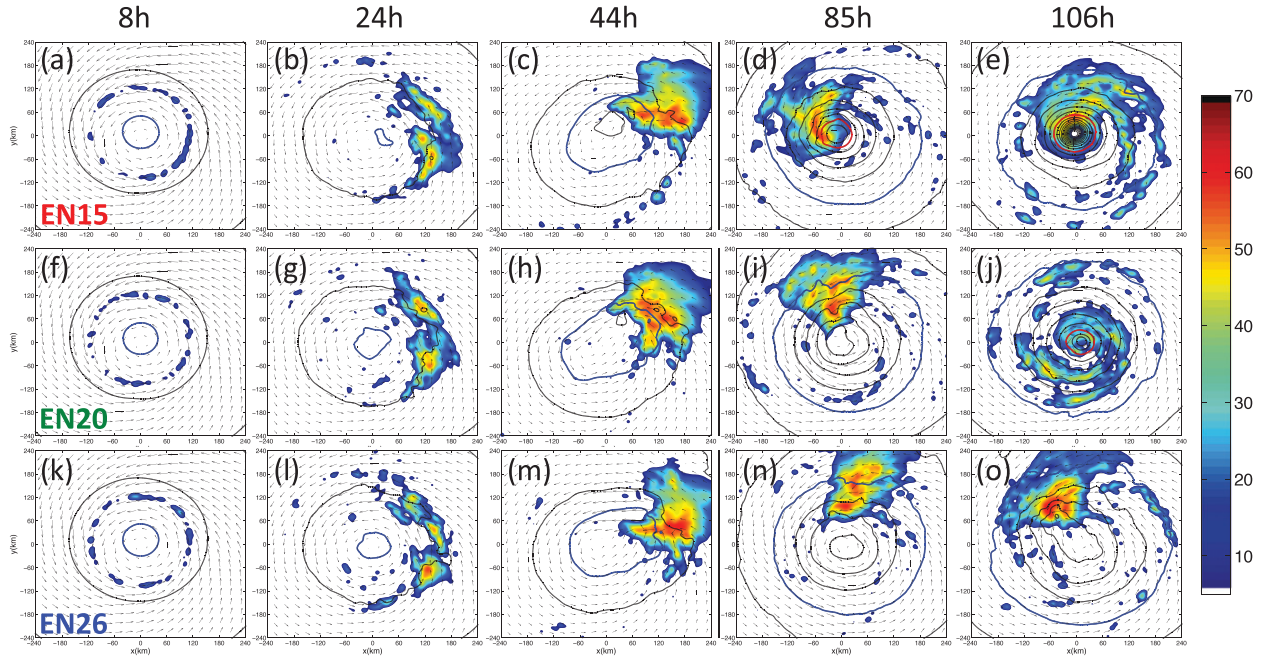
FIG. 3. The 10-m surface wind vectors, mean sea level pressure (black contours every 2 hPa; thick blue contour for 1010 hPa and thick red contour for 1000 hPa), and column-maximum reflectivity (dB*Z*; color filled) for ensemble members (a)–(e) EN15, (f)–(j) EN20, and (k)–(o) EN26 in SH5 at (from left to right) 8, 24, 44, 85, and 106 h.

beyond the scope of this study to ascertain the precise reason(s) for the greater intensity uncertainty in NSM08.

It is also worth noting that there is a secondary peak of ensemble spread in experiments with 3 and 5 m s^{-1} vertical shear during the initial formation stage of the tropical cyclones (from 42 to 48 h). This is the initial formation/development stage of all members in both ensemble experiments, when the TC reaches tropical storm intensity ($\sim$17 m s^{-1}). This early development is notably absent in the experiments with 0 or 1 m s^{-1} mean shear, neither of which has a secondary peak of ensemble spread during the first 48 h. Although it is beyond the scope of the current paper, the difference in the formation and early development of tropical cyclones between experiments with moderate versus no or minimal shear suggests that the presence of moderate shear is capable of facilitating the earlier formation/ development of tropical cyclones (e.g., Molinari and Vollaro 2010; Nolan and McGauley 2012), despite the fact that the eventual maximum intensity is somewhat smaller.

b. Forecast divergence during RI

To understand how small initial moisture perturbations cause the large forecast uncertainty of tropical cyclone intensity in a sheared environment, we examine three example members in SH5 (which has the largest ensemble spread), with EN15 the earliest intensifier,

EN20 near the middle, and EN26 the slowest (highlighted in Fig. 2d). Figure 3 shows the mean sea level pressure (MSLP) along with the simulated column-maximum reflectivity for each of these three members at select times. At 8 h, convection begins to develop near the radius of maximum wind, nearly uniformly in all directions around the incipient storms. By 24 h, under the influence of the 5 m s^{-1} westerly shear, the strongest convection is concentrated to the eastern (downshear) side, and there is no apparent difference in intensity among the different members. The strongest convection further rotates to the downshear-left quadrant of the TCs at 44 h. By now the minimum SLP of EN15 has become slightly lower than the other two members. At 85 h, after the strongest convection in EN15 has moved into the upshear-left quadrant of the storm, it begins to become more axisymmetric and the RI commences within a few hours. By this time, the strongest convection in EN20 has just moved to the upshear-left quadrant, and convection remains in the downshear-left quadrant for EN26. By 106 h, EN15 has developed into a mature hurricane, while convection in EN20 begins to be axisymmetrized just before rapid intensification, 21 h later than in EN15. At this time, the strongest convection in EN26 is still in the upshear-left quadrant, and axisymmetrization and rapid intensification does not start until after 132 h (not shown).
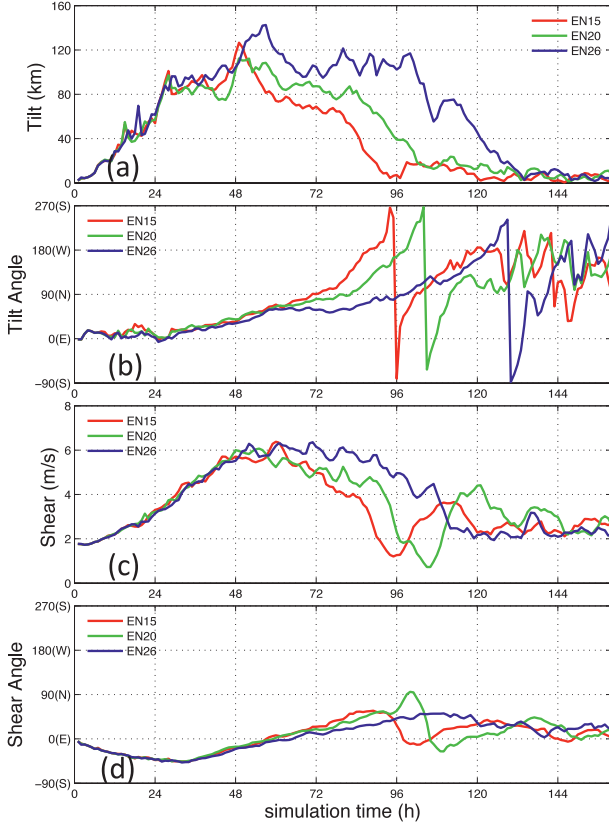
FIG. 4. Time evolution of the direction and magnitude of the storm-center tilt and the local vertical wind shear. (a) Tilt magnitude; (b) tilt angle; (c) shear magnitude; (d) shear angle for ensemble members EN15 (red), EN20 (green), and EN26 (blue) in SH5.

To further understand how and when these three members start to differ systematically, and what results in the loss of predictability in experiment SH5, we examine the time evolution of the direction and magnitude of the local vertical wind shear and the storm-center tilt in Fig. 4. The tilt and shear vectors along with the maximum reflectivity and MSLP for each member at select times are shown in Fig. 5. Calculation of the tilt and shear follows that of Rappin and Nolan (2012), except that we use the weighted horizontal circulation center instead of the Ertel potential vorticity center that they used. Tilt is defined as the difference between the 900- and 500-hPa circulation center position, while the local vertical shear is calculated using the difference between horizontal winds at the 900- and 500-hPa levels averaged within a 300-km-radius circle centered on the 700-hPa circulation center (the environmental shear between these two levels in SH5 is about 2 m s^{-1} initially; Fig. 1).

As shown in Fig. 4, each ensemble member first undergoes an increase in the magnitude of both tilt and

local vertical shear, owing to the effect of environmental shear on the incipient storm. Except for the direction of the shear, there are large differences in the evolution of both the tilt and shear vectors that lead to subsequent differences in the timing of rapid intensification among different members. The systematic difference among members first starts in the tilt magnitude around 52–60 h (Fig. 4a), just before the local shear in all three members reaches a maximum. This divergence in tilt magnitude is apparently due to the randomness of moist convection that leads to stronger convective bursts closer to the primary vortex center in EN15 than in EN20, both of which are stronger than EN26. Evidence for this can be seen in Figs. 6a–c, which shows the time evolution of the azimuthal average of the vertically integrated diabatic heating rate (only positive values are summed) as a function of radial distance. From around 52–60 h, a strong burst of convection induces expansive diabatic heating within a radial range of 90–110 km just outside the radius of 10-m maximum wind (RMW) in EN15 (Fig. 6a), which is stronger in magnitude and/or areal coverage than in both EN20 and EN26 (Figs. 6b,c).[2] This strong burst of convection leads to an immediate enhancement of potential vorticity (PV) in the middle troposphere around the RMW in EN15 (Fig. 6d) and to a lesser degree in EN20 (Fig. 6e). There is also some enhancement of diabatic heating just outside the RMW (Fig. 6c) and subsequent enhancement of midlevel PV (Fig. 6f) in EN26, but with a much weaker amplitude, and also 6–12 h later than in EN15 and EN20.

Subsequently, tilt angle and shear magnitude among members begin to differ at around 60 h (Figs. 4b,c). After the tilt angle reaches 90° to the left of the environmental shear (Fig. 4) at around 71, 79, and 99 h in EN15, EN20, and EN26 (Figs. 5a,g,n), respectively, the tilt vector moves cyclonically at a faster angular speed while both tilt and local shear decrease rapidly in magnitude, reaching minima at around 94 (Fig. 5c), 102 (Fig. 5j), and 133 h (not shown), respectively. The rapid intensification of the tropical cyclone immediately follows

---

[2] It is worth noting that there is also another earlier episode of convective burst from 36 to 48 h that differs greatly among the three ensemble members, as seen by the large difference in diabatic heating (Figs. 6a–c). During this earlier episode, EN20, instead of EN15, has the strongest convective burst just outside the RMW, both of which are stronger than EN26. In other words, the strong burst of convection itself may not be sufficient for the rapid intensification to occur. It is possible that this earlier difference in convection may have conditioned the difference in the subsequent burst of convection from 52 to 60 h. There is hardly any noticeable difference in the initial burst of convective heating among the three members during 12–24 h.
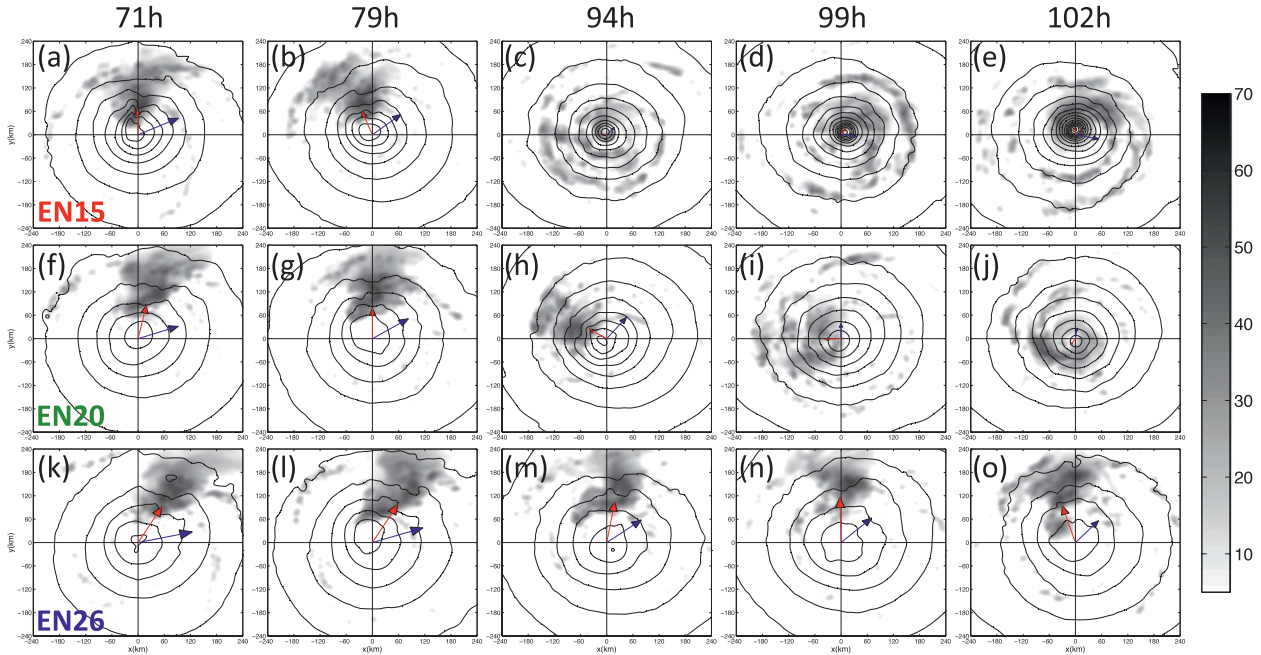
FIG. 5. Mean sea level pressure (contoured every 2 hPa), column-maximum reflectivity (dBZ, gray shading), tilt vector (red arrow), and shear vector (blue arrow) for ensemble members (a)–(e) EN15, (f)–(j) EN20, and (k)–(o) EN26 in SH5 at (from left to right) 71, 79, 94, 99, and 102 h.

after the vortex tilt and local shear reach their respective minima (Fig. 2d). The evolution of the shear and tilt vectors in each ensemble member before rapid intensification is consistent with the precession process by which the tropical cyclone vortex interacts with the environmental shear, as discussed in Rappin and Nolan (2012). The importance of the precession of tilt in TCs is also shown in Davis et al. (2008). Consistent with Figs. 2d and 3, Fig. 5 also further demonstrates the strong divergence of the TC structure and intensity among different ensemble members right before and during their rapid intensification. This again exemplifies the intrinsic limit of predictability of TCs under moderate environmental shear. Future research will extend this study to further explore the effects of even stronger vertical wind shear and other environmental inhomogeneities on the predictability of TCs.

c. Forecast divergence after RI and partial eyewall replacement cycle (ERC)

Now we come back to examine why the 1 m s^{-1} shear ensemble experiment SH1 has the largest ensemble spread among all experiments after the rapid intensification completes. We again select three exemplary ensemble members from SH1, with EN13 the strongest, EN18 near the middle, and EN24 the weakest during the post-RI period (highlighted in Fig. 2b). Figure 7 shows the time evolution of the azimuthal average of the radial

distribution of the 10-m tangential winds, the 500-hPa vertical velocity, and the column-integrated diabatic heating rate (positive values only). The simulations of these three members in Fig. 7 extend 48 h beyond what are present in Fig. 2b.

The intensity divergence of EN13, EN18, and EN24 after the RI completion is apparently associated with differences in the timing and strength/degree of their respective ERCs, as shown clearly in the different evolutions of vertical velocity and diabatic heating rate, and to a lesser degree in the surface tangential winds (Fig. 7). In the azimuthally averaged fields, both EN18 and EN24 (but not EN13) develop a coherent secondary maximum of upward vertical motion (Figs. 7e,f) and positive diabatic heating (Figs. 7h,i) starting at a radial range of 120–150 km (far outside the primary eyewall updraft), which is characteristic of a secondary eyewall formation (SEF).

While the exact processes that lead to the SEF/ERC remain a very active area of research (e.g., Terwey and Montgomery 2008; Qiu and Tan 2010; Huang et al. 2012; Rozoff et al. 2012; Fang and Zhang 2012), it is evident from Fig. 7 that prior to the formation of this secondary eyewall, there is more widespread convective activity radiating away from the primary eyewall in both EN18 and EN24 than EN13. The formation of this secondary eyewall (at around 168 h for EN24 and around 196 h for EN18) leads to the weakening of the radial inflow to the
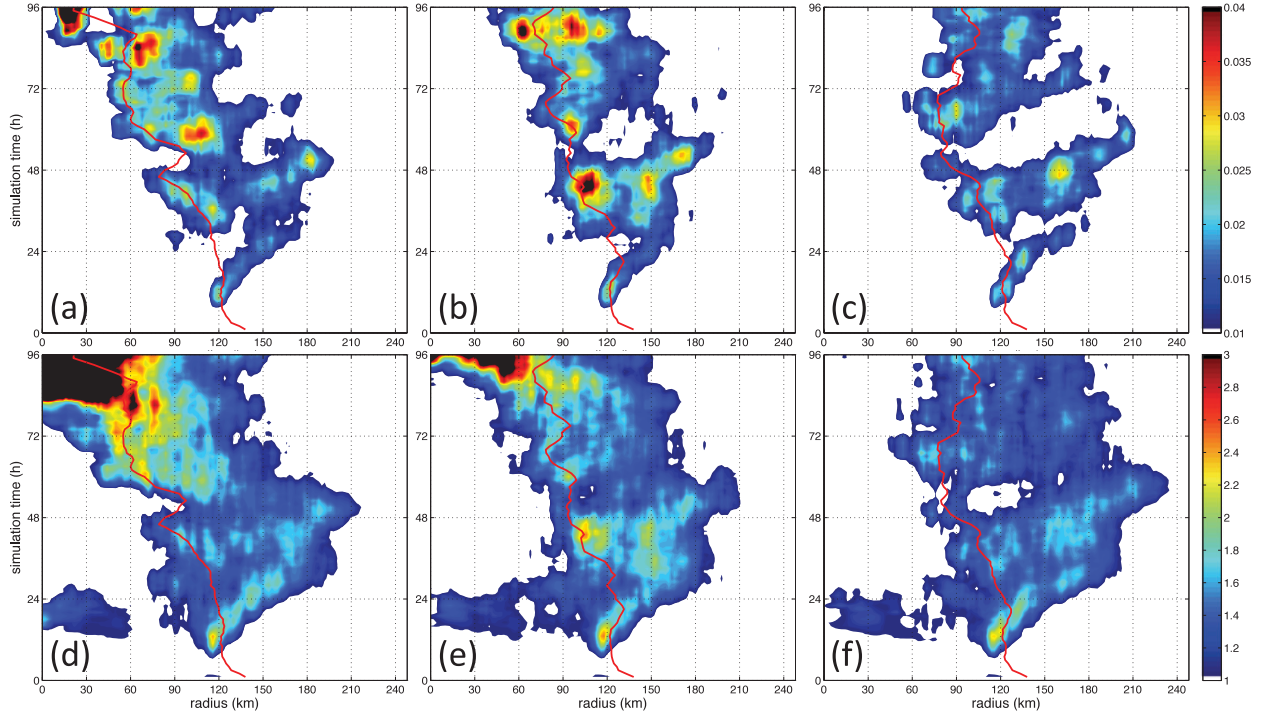
FIG. 6. Time evolution of azimuthally averaged (a)–(c) column-integrated positive-only diabatic heating rate (K s^{-1}) and (d)–(f) 500-hPa positive potential vorticity [potential vorticity units (PVU)] for ensemble members (left) EN15, (middle) EN20, and (right) EN26 in SH5. The red line denotes the radius of maximum 10-m tangential wind in each member.

primary eyewall (not shown). This subsequently leads to the weakening of the primary-eyewall convection (Figs. 7e–f, h–i) and thus the intensity of the tropical cyclone. The formation of this secondary eyewall also leads to the radial expansion of the maximum tangential winds in both EN24 and EN18. However, the secondary eyewall appears to be insufficient to establish a secondary tangential wind maximum during its inward contraction before its eventual merger with the primary eyewall (and thus it is labeled as a partial ERC). Nevertheless, it is apparent from Figs. 7a–c that this partial ERC, and the differences in its timing, both of which ultimately originate from the randomness of moist convection, can substantially influence the predictability of the structure and intensity of the tropical cyclones.

It is worth noting that the partial ERC is not unique to the 1 m s^{-1} shear ensemble experiment SH1. For instance, all three of the ensemble members in SH5 discussed in section 3b (i.e., EN15, EN20, and EN26) undergo a similar partial ERC after the completion of RI (not shown), but for reasons that are beyond the scope of the current study, the differences in the timing and degree of the ERC among these SH5 ensemble members is considerably smaller and thus has a smaller influence on the storm intensity.

4. Concluding remarks

This study explores the effect of vertical wind shear on the predictability of tropical cyclone intensity during different stages of the TC life cycle, through cloud-resolving ensemble simulations using the Weather Research and Forecasting (WRF) model. It is found that the predictability of tropical cyclone intensity can be significantly influenced by the environmental vertical wind shear, especially during the formation and rapid intensification stage. The larger the vertical wind shear, the larger the uncertainty in the intensity forecast, primarily because of the difference in the timing of rapid intensification.

In the presence of vertical wind shear, small-scale, small-amplitude random initial noise may lead to changes in the onset and ending of rapid intensification by as much as 1–2 days, through the randomness and chaotic nature of moist convection. Upscale error growth from differences in moist convection first alters the tilt amplitude and angle of the incipient tropical storms, which later leads to significant differences in the timing of precession and vortex alignment. During the precession process, both the vertical tilt of the storm and the effective (local) vertical wind shear are considerably decreased after the tilt angle reaches 90° to the
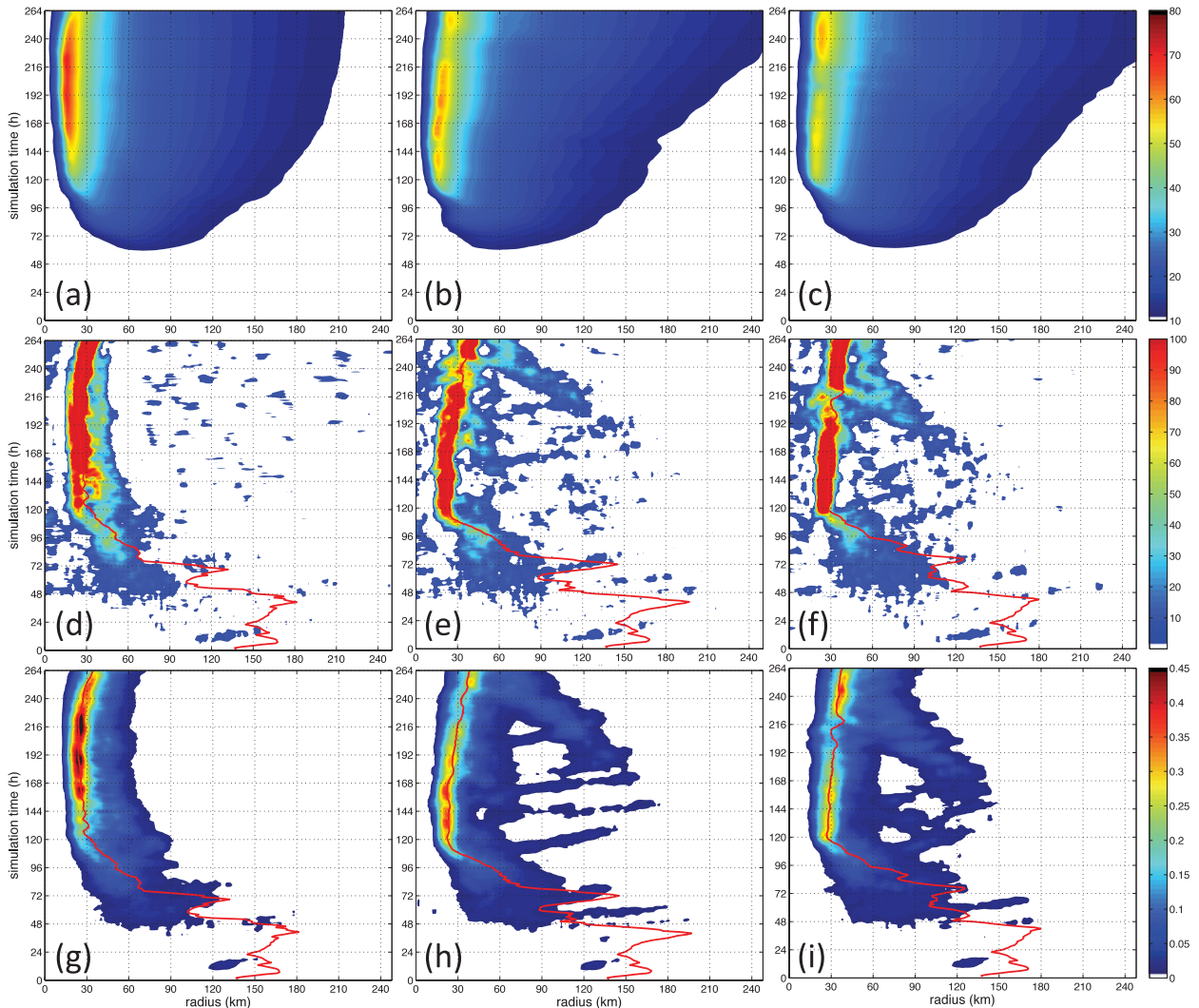
FIG. 7. Time evolution of azimuthally averaged (a)–(c) tangential 10-m wind (m s^{-1}), (d)–(f) 500-hPa vertical wind (cm s^{-1}), and (g)–(i) column-integrated positive-only diabatic heating rate (K s^{-1}) for ensemble members (left) EN13, (middle) EN18, and (right) EN24. The red line denotes the radius of maximum 10-m tangential wind in each member.

left of the environmental shear. The tropical cyclones rapidly intensify immediately after the tilt and the effective local shear reach their respective minima. The time at which this occurs is different in each member, with the differences among members becoming larger with increasing vertical wind shear, consistent with the recent study of Rappin and Nolan (2012). In other words, the predictability of tropical cyclone intensity during the formation and rapid intensification stages is intrinsically more limited in the presence of stronger vertical wind shear. Further, our study also shows that the uncertainty due to small random initial-condition error in NSM08 may have been overestimated owing to the poor model resolution/physics that they used.

REFERENCES

Cangialosi, J. P., and J. L. Franklin, 2012: 2011 National Hurricane Center verification report. Tropical Prediction Center, National Hurricane Center, National Center for Environmental

Prediction, National Weather Center, NOAA, 76 pp. [Available at http://origin.www.nhc.noaa.gov/verification/pdfs/Verification_2011.pdf.]

Davis, C. A., S. C. Jones, and M. Riemer, 2008: Hurricane vortex dynamics during Atlantic extratropical transition. *J. Atmos. Sci.,* **65,** 714–736.

Deng, Q., L. Smith, and A. J. Majda, 2012: Tropical cyclogenesis and vertical shear in a moist Boussinesq model. *J. Fluid Mech.,* **706,** 384–412.

Dudhia, J., and Coauthors, 2008: Prediction of Atlantic tropical cyclones with the Advanced Hurricane WRF (AHW) model. Preprints, *28th Conf. on Hurricanes and Tropical Meteorology,* Orlando, FL, Amer. Meteor. Soc., 18A.2. [Available online at https://ams.confex.com/ams/28Hurricanes/techprogram/paper_138004.htm.]

Dunion, J. P., and C. S. Marron, 2008: A reexamination of the Jordan mean tropical sounding based on awareness of the Saharan air layer: Results from 2002. *J. Climate,* **21,** 5242–5253.

Fang, J., and F. Zhang, 2012: Effect of beta shear on simulated tropical cyclones. *Mon. Wea. Rev.,* **140,** 3327–3346.

Hong, S.-Y., and J.-O. J. Lim, 2006: The WRF single-moment 6-class microphysics scheme (WSM6). *J. Korean Meteor. Soc.,* **42,** 129–151.

——, Y. Noh, and J. Dudhia, 2006: A new vertical diffusion package with an explicit treatment of entrainment processes. *Mon. Wea. Rev.,* **134,** 2318–2341.

Huang, Y.-H., M. T. Montgomery, and C.-C. Wu, 2012: Concentric eyewall formation in Typhoon Sinlaku (2008). Part II: Axisymmetric dynamical processes. *J. Atmos. Sci.,* **69,** 662–674.

Molinari, J., and D. Vollaro, 2010: Rapid intensification of a sheared tropical storm. *Mon. Wea. Rev.,* **138,** 3869–3885.

Nguyen, V. S., R. K. Smith, and M. T. Montgomery, 2008: Tropical-cyclone intensification and predictability in three dimensions. *Quart. J. Roy. Meteor. Soc.,* **134,** 563–582.

Nolan, D. S., 2011: Evaluating environmental favorableness for tropical cyclone development with the method of point downscaling. *J. Adv. Model. Earth Syst.,* **3,** M08001, doi:10.1029/2011MS000063.

——, and M. G. McGauley, 2012: Tropical cyclogenesis in wind shear: Climatological relationships and physical processes.

Cyclones: Formation, Triggers and Control, K. Oouchi and H. Fudeyasu, Eds., Nova Science Publishers, 1–34.

Qiu, X., and Z.-M. Tan, 2010: The role of vortex Rossby waves in hurricane secondary eyewall formation. *Mon. Wea. Rev.,* **138,** 2092–2109.

Rappin, E. D., and D. S. Nolan, 2012: The effect of vertical shear orientation on tropical cyclogenesis. *Quart. J. Roy. Meteor. Soc.,* **138,** 1035–1054, doi:10.1002/qj.977.

Rozoff, C. M., D. S. Nolan, J. P. Kossin, F. Zhang, and J. Fang, 2012: The roles of an expanding wind field and inertial stability in tropical cyclone secondary eyewall formation. *J. Atmos. Sci.,* **69,** 2621–2643.

Sippel, J. A., and F. Zhang, 2008: A probabilistic analysis of the dynamics and predictability of tropical cyclogenesis. *J. Atmos. Sci.,* **65,** 3440–3459.

——, and ——, 2010: Factors affecting the predictability of Hurricane Humberto (2007). *J. Atmos. Sci.,* **67,** 1759–1778.

Tang, B., and K. Emanuel, 2010: Midlevel ventilation's constraint on tropical cyclone intensity. *J. Atmos. Sci.,* **67,** 1817–1830.

Terwey, W. D., and M. T. Montgomery, 2008: Secondary eyewall formation in two idealized, full-physics modeled hurricanes. *J. Geophys. Res.,* **113,** D12112, doi:10.1029/2007JD008897.

Uhlhorn, E. W., and D. S. Nolan, 2012: Observational undersampling in tropical cyclones and implications for estimated intensity. *Mon. Wea. Rev.,* **140,** 825–840.

Zhang, F., and J. A. Sippel, 2009: Effects of moist convection on hurricane predictability. *J. Atmos. Sci.,* **66,** 1944–1961.

——, C. Snyder, and R. Rotunno, 2002: Mesoscale predictability of the "surprise" snowstorm of 24–25 January 2000. *Mon. Wea. Rev.,* **130,** 1617–1632.

——, ——, and ——, 2003: Effects of moist convection on mesoscale predictability. *J. Atmos. Sci.,* **60,** 1173–1185.

——, N. Bei, R. Rotunno, C. Snyder, and C. C. Epifanio, 2007: Mesoscale predictability of moist baroclinic waves: Convection-permitting experiments and multistage error growth dynamics. *J. Atmos. Sci.,* **64,** 3579–3594.

——, Y. Weng, J. F. Gamache, and F. D. Marks, 2011: Performance of cloud-resolving hurricane initialization and prediction during 2008–2010 with ensemble data assimilation of inner-core airborne Doppler radar observations. *Geophys. Res. Lett.,* **38,** L15810, doi:10.1029/2011GL048469.